NASA TECHNICAL NOTE

NASA TN D-4614

C. 1

NASA TN D-4614

BODY ROTATION EFFECTS ON MELTING ABLATION

by Thomas H. Cochran and Simon Ostrach

Lewis Research Center
Cleveland, Ohio

NATIONAL AERONAUTICS AND SPACE ADMINISTRATION • WASHINGTON, D. C. • JUNE 1968

NASA TN D-4614

BODY ROTATION EFFECTS ON MELTING ABLATION

By Thomas H. Cochran and Simon Ostrach

Lewis Research Center
Cleveland, Ohio

NATIONAL AERONAUTICS AND SPACE ADMINISTRATION

For sale by the Clearinghouse for Federal Scientific and Technical Information
Springfield, Virginia 22151 – CFSTI price $3.00

CONTENTS

BODY ROTATION EFFECTS ON MELTING ABLATION

by Thomas H. Cochran and Simon Ostrach*

Lewis Research Center

SUMMARY

The effects of rotation on the ablation of an axisymmetric body composed of a highly viscous material and subject to deceleration in an airstream were studied analytically and experimentally. The tests were conducted so that a parameter representing the importance of rotation effects and which was obtained from a nondimensionalization of the governing equations was varied from 0 to 4.2.

The results indicate that, although rotation had no effect on the ablation process in the vicinity of the stagnation point of the body, significant changes in the character of the generated waves and in the flange were caused by rotation. Liquid was thrown from the body in the vicinity of the flange when the spin parameter was 0.88 or greater.

INTRODUCTION

With the advent of space travel, the need has arisen for the protection of payloads from the high heat fluxes encountered during reentry into the Earth's Atmosphere. Solutions to this problem have centered around the use of external shields which are sacrificed in an ablation process in order to protect the vehicle interior. For ballistic applications which have relatively short-time high-heat-intensity reentry characteristics, ablative materials that sublime have been of greatest interest. However, for the longer time, lower heat intensity reentry environments which a manned spacecraft may encounter, ablative materials can melt before they vaporize. Therefore, numerous research programs, which are discussed in the following section, have been initiated to study the fluid dynamics and heat transfer of thin melt layers.

---

*Professor of Engineering, Head of Division of Fluid, Thermal, and Aerospace Sciences, Case Institute of Technology, Cleveland, Ohio.

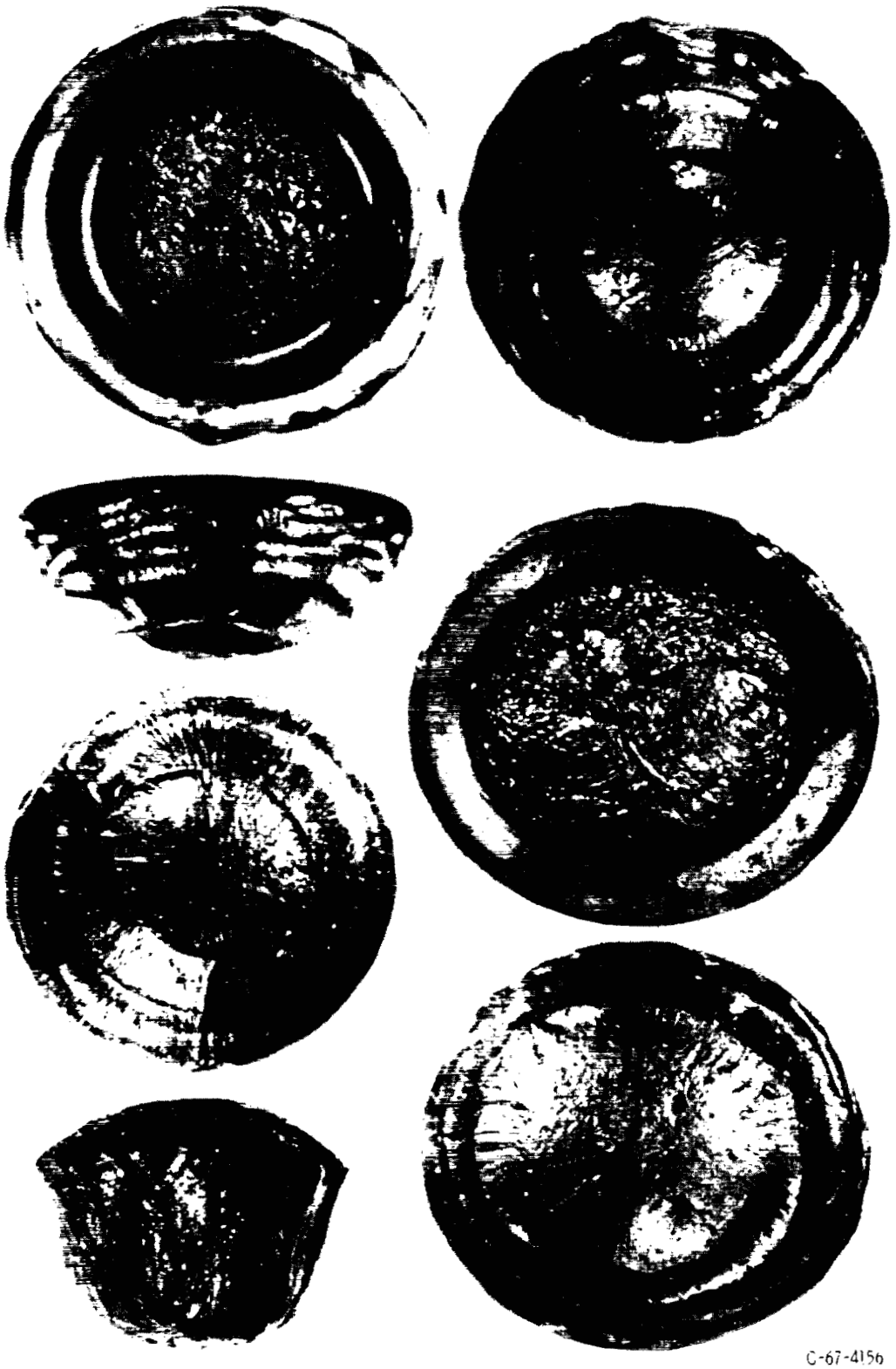

C-67-4156

Figure 1. - External structure of tektites.

Another area in which melting ablation has become of significance is in the explanation of tektites. These small (about 2 cm in diam) button-shaped glassy bodies (see fig. 1) have been found over large areas at numerous sites around the world and bear no geological resemblance to their surroundings. On the surface of some of these objects, such as those found in Australia, are ring-shaped waves and an equatorial flange. Chapman (ref. 1), and Ostrach (ref. 2) have found that this distinctive appearance can be produced on bodies ablated in a wind tunnel. Based on such aerodynamic tests and exhaustive geometric and structural investigations, Chapman has proposed that tektites are extraterrestrial, having ablated during entry into the Earth's atmosphere. Further, by measuring the amount of ablation at the stagnation point and the spacing of the ring waves, he has obtained trajectory information that has led him to confirm the suggestion that the origin of tektites is the moon. O'Keefe (refs. 3 and 4) agrees with a lunar origin. However, he believes that the individual tektites did not come directly from the moon as Chapman has proposed but were torn from a larger body as it passed through the Earth's atmosphere. Regardless of their nature before reaching the Earth, tektites provide a convenient model and standard for melting ablation research.

A possible condition imposed on a body entering the atmosphere is that of spinning. Chapman (ref. 1) suggests that tektites rotate during their ablation; however, no mention is made of expected rates or effects on the ablation process. It is possible that rotation effects (centrifugal and coriolis forces) could play an important role in the dynamics of a melt layer, and hence the ablation process. This suggests that the variation in the amount of ablation apparent on different tektites may be attributed to rotation rather than trajectory characteristics.

This report presents the results of an investigation of the effects on melting ablation of rotation about the major axis of a body of revolution similar to that of a tektite. The problem was, first, treated analytically to obtain the pertinent governing equations and then experimentally to measure the effects of rotation on the ablation process. Test models were spun over a wide range of speeds (0 to 400 rpm) in an effort to obtain a clear picture of rotation effects on the melt.

PREVIOUS ABLATION WORK

The early work in ablation was keyed to design criteria because of the need for immediate information. Approximate analysis and experimentation were used to provide the engineer with the necessary tools to treat the problem grossly. Adams has provided a survey of these design techniques in reference 5.

Early attempts to treat aerodynamic ablation in a more exact manner were confined to the stagnation region. Sutton's work in reference 6 is considered a classic of these initial efforts because he was able to show the importance of the melt layer in the ablation process. However, he compromised his solution by neglecting transient effects.

A significant advance in defining melting ablation phenomena was achieved by Ostrach, Goldstein, and Hamman in reference 7. Here, the problem was approached in a general form by including transient effects and vehicle deceleration. Their solution, which was carried out around the body as well as at the stagnation point, showed the importance of body forces on the melt and predicted a wave-like behavior. However, only a single wave was indicated, rather than the repeated waves found on the tektites. Also, the solution was essentially quasi-steady.

McConnell (ref. 8) extended Ostrach's work by applying a perturbation analysis to the early stages of ablation where conduction dominates convection. He also improved Ostrach's quasi-steady solution by generalizing the boundary condition. Comparison of his theoretical results with experimental data taken with asphalt spheres in a wind tunnel indicated good agreement.

In recent work in this problem, Chen (ref. 9) has extended the detailed analysis of the liquid-layer equations by Ostrach and McConnell to include the gas-boundary-layer equations. By considering the coupling of the gas and liquid equations at their interface, he has been able to obtain pertinent reference quantities which permit a more rigorous nondimensional treatment of the governing equations. This approach to the problem also improves the validity of boundary conditions at the interface.

The value of Chen's analysis has been demonstrated to some extent by the work of Edling (ref. 10). He investigated the characteristics of waves generated on an ablating flat plate for several different materials. A correlation of the results was accomplished through an ablation parameter which was derived by Chen and predicted earlier by Ostrach and McConnell (ref. 2). This parameter relates the rate at which a substance melts to the incident heating rate.

ANALYSIS

Melting Ablation Model

The mathematical model assumed is that of an axisymmetric body composed of a material which, when in a liquid state, has a viscosity that is highly temperature-dependent. The thermal conductivity, specific heat, and density of the material will be considered to be independent of temperature. The body is assumed to decelerate at a constant rate in the atmosphere and is subject to heating sufficient to cause a layer of

melted material to flow along the surface. Because of the viscous nature of the material, the layer is very thin compared with the body size, and no distinct liquid-solid interface is identifiable. The flow is driven by aerodynamic, gravity, and rotational forces. Evaporation of material is neglected.

A schematic drawing of the model is shown in figure 2. Since the liquid layer is thin compared with the radius of curvature of the body, a Cartesian coordinate system is chosen normal to and along the liquid-gas interface. The x-axis is along the interface meridionally, the y-axis is perpendicular to the interface, and the z-axis is along the interface azimuthally. The coordinate system is fixed at the liquid-gas interface and is rotating at a constant rate equal to that of the solid portion of the body. It is assumed

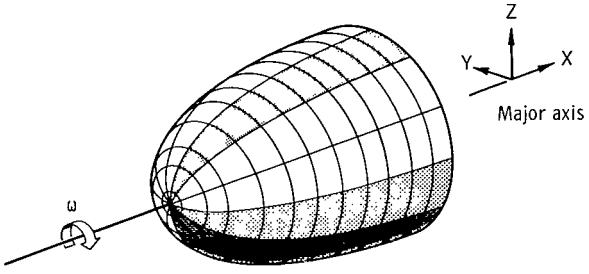

(a) Three-dimensional view.

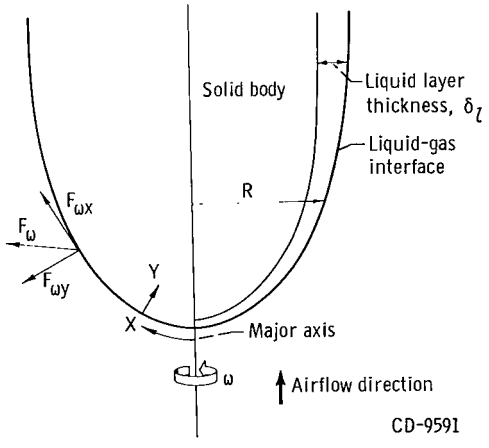

(b) Cutaway view.

Figure 2. - Mathematical ablation model.

that acceleration terms associated with the unsteady motion of the interface relative to the body are negligible.

Governing Liquid Equations

Dimensional equations. - The equations governing the motion of the liquid layer are:

Continuity:

$$\frac{\partial}{\partial X}(RU) + \frac{\partial}{\partial Y}(RV) = 0 \tag{1}$$

Momentum:

$$\rho_l \left[\frac{\partial U}{\partial \bar{t}} + U \frac{\partial U}{\partial X} + V \frac{\partial U}{\partial Y} - A \sqrt{1 - \left(\frac{dR}{dX}\right)^2} - \left(\frac{\overline{W}^2}{R} + 2\overline{W}\omega + \omega^2 R \right) \frac{dR}{dX} \right]$$

$$= - \frac{\partial P}{\partial X} + \frac{\partial}{\partial Y} \left[\overline{\mu}_l \left(\frac{\partial V}{\partial X} + \frac{\partial U}{\partial Y} \right) \right] + 2 \frac{\partial}{\partial X} \left(\overline{\mu}_l \frac{\partial U}{\partial X} \right) \tag{2}$$

$$\rho_l \left[\frac{\partial V}{\partial \bar{t}} + U \frac{\partial V}{\partial X} + V \frac{\partial V}{\partial Y} - A \frac{dR}{dX} + \left(\frac{\overline{W}^2}{R} + 2\overline{W}\omega + \omega^2 R \right) \sqrt{1 - \left(\frac{dR}{dX}\right)^2} \right]$$

$$= - \frac{\partial P}{\partial Y} + \frac{\partial}{\partial X} \left[\overline{\mu}_l \left(\frac{\partial U}{\partial Y} + \frac{\partial V}{\partial X} \right) \right] + 2 \frac{\partial}{\partial Y} \left(\overline{\mu}_l \frac{\partial V}{\partial Y} \right) \tag{3}$$

$$\rho_l \left[\frac{\partial \overline{W}}{\partial \bar{t}} + U \frac{\partial \overline{W}}{\partial X} + V \frac{\partial \overline{W}}{\partial Y} + 2U\omega \frac{dR}{dX} - 2V\omega \sqrt{1 - \left(\frac{dR}{dX}\right)^2} \right] = \frac{\partial}{\partial X} \left(\overline{\mu}_l \frac{\partial \overline{W}}{\partial X} \right) + \frac{\partial}{\partial Y} \left(\overline{\mu}_l \frac{\partial \overline{W}}{\partial Y} \right) \tag{4}$$

Energy (neglecting thermal expansion):

$$\rho_l (C_p)_l \left(\frac{\partial T}{\partial \bar{t}} + U \frac{\partial T}{\partial X} + V \frac{\partial T}{\partial Y} \right) = k_l \left(\frac{\partial^2 T}{\partial X^2} + \frac{\partial^2 T}{\partial Y^2} \right) + \Phi \tag{5}$$

where Φ is the dissipation function and is expressed as

$$\Phi + \overline{\mu}_l \left[2\left(\frac{\partial U}{\partial X}\right)^2 + 2\left(\frac{\partial V}{\partial Y}\right)^2 + 2\,\frac{\partial U}{\partial Y}\,\frac{\partial V}{\partial X} + \left(\frac{\partial U}{\partial Y}\right)^2 + \left(\frac{\partial V}{\partial X}\right)^2 + \left(\frac{\partial \overline{W}}{\partial Y}\right)^2 + \left(\frac{\partial \overline{W}}{\partial X}\right)^2 \right] \tag{6}$$

Constitutive relation:

$$\frac{\overline{\mu}_l}{\overline{\mu}_{il}} = \left(\frac{T - T_\infty}{T_i - T_\infty}\right)^{-N} \tag{7}$$

(All symbols are defined in appendix A.)

In writing these equations, the tangential velocity due to spinning is taken to be independent of y. The error involved in assuming this is negligible because of the thinness of the liquid layer. Deceleration, coriolis, and centrifugal terms arise in the transformation from a stationary coordinate system to the one fixed at the liquid-gas interface.

Nondimensionalization. - Simplification of the equations is accomplished by a nondimensional technique. By careful selection of characteristic values for the variables, the relative importance of the different terms in the equations can be assessed. The nondimensional variables are as follows:

$$x = \frac{X}{L}, \qquad y = \frac{Y}{\delta_l L}, \qquad \mu = \frac{U}{U_{ref}}, \qquad v = \frac{V}{\Delta_1 U_{ref}}, \qquad w = \frac{\overline{W}}{\Delta_2 U_{ref}}$$

$$\mu_l = \frac{\overline{\mu}_l}{\overline{\mu}_{il}}, \qquad t = \frac{\bar{t}}{\sigma}, \qquad r = \frac{R}{L}, \qquad y_T = \frac{Y}{e_l L}, \qquad p = \frac{P}{\rho_g U_{-\infty}^2}$$

$$\theta = \frac{T - T_\infty}{T_i - T_\infty}$$

Of the characteristic values, the scaling parameter for the liquid velocity layer thickness δ_l, the reference velocity U_{ref}, the characteristic time value σ, the scaling parameter for the liquid thermal layer thickness e_l, the scaling parameter for the velocity normal to the liquid-gas interface Δ_1, the temperature at the liquid-gas interface T_i, and the scaling parameter for the velocity in the azimuthal direction Δ_2 are unknown

and must be determined from an order-of-magnitude analysis of the nondimensional equations and boundary conditions. Chen (ref. 9) evaluated δ_l, U_{ref}, σ, e_l, T_i, and Δ_1, and his analysis is presented in detail in appendix B. The remaining parameter Δ_2 must be obtained from the equation of motion for the azimuthal direction. This equation in nondimensional form is

$$\left(Re_l \delta_l^2 \Delta_2\right)\left(\frac{\partial w}{\partial t} + u\frac{\partial w}{\partial x} + v\frac{\partial w}{\partial y}\right) + 2\left(Re_\Omega \delta_l^2\right)\left(u\frac{dr}{dx} - \delta_l v\sqrt{1 - \left(\frac{dr}{dx}\right)^2}\right)$$

$$= \Delta_2\left[\frac{\partial}{\partial y}\left(\mu_l \frac{\partial w}{\partial y}\right) + \delta_l^2 \frac{\partial}{\partial x}\left(\mu_l \frac{\partial w}{\partial x}\right)\right] \tag{8}$$

Assuming that any motion of the liquid in the aximuthal direction relative to the spinning reference system is driven by coriolis forces and opposed by viscous forces results in

$$\Delta_2 = 2\left(Re_\Omega \delta_l^2\right) \tag{9}$$

After inserting the new variables and gathering terms, the equations are

$$\frac{\partial}{\partial x}(ru) + \frac{\partial}{\partial y}(rv) = 0 \tag{10}$$

$$\left(Re_l \delta_l^2\right)\left(\frac{\partial u}{\partial t} + u\frac{\partial u}{\partial x} + v\frac{\partial u}{\partial y}\right) - 4\left(Re_l Re_\Omega^2 \delta_l^6\right)\frac{w^2}{r}\frac{dr}{dx} - (N_s) r \frac{dr}{dx} - 4\left(Re_\Omega^2 \delta_l^4\right) w \frac{dr}{dx}$$

$$+ (N_p)\left(\frac{\partial p}{\partial x} - g\sqrt{1 - \left(\frac{dr}{dx}\right)^2}\right) = \frac{\partial}{\partial y}\left[\mu_l\left(\delta_l^2 \frac{\partial v}{\partial x} + \frac{\partial u}{\partial y}\right)\right] + 2\delta_l^2 \frac{\partial}{\partial x}\left(\mu_l \frac{\partial u}{\partial x}\right) \tag{11}$$

$$\left(\mathrm{Re}_l\,\delta_l^4\right)\left(\frac{\partial v}{\partial t}+u\,\frac{\partial v}{\partial x}+v\,\frac{\partial v}{\partial y}\right)+4\left(\mathrm{Re}_l\,\mathrm{Re}_\Omega^2\,\delta_l^7\right)\,\frac{w^2}{r}\,\sqrt{1-\left(\frac{dr}{dx}\right)^2}+(N_s\delta_l)\,r\,\sqrt{1-\left(\frac{dr}{dx}\right)^2}$$

$$+4\left(\mathrm{Re}_\Omega^2\,\delta_l^5\right)\,w\,\sqrt{1-\left(\frac{dr}{dx}\right)^2}+(N_p)\left(\frac{\partial p}{\partial y}-\delta_l\,g\,\frac{dr}{dx}\right)$$

$$=\delta_l^2\left\{2\,\frac{\partial}{\partial y}\left(\mu_l\,\frac{\partial v}{\partial y}\right)+\frac{\partial}{\partial x}\left[\mu_l\left(\frac{\partial u}{\partial y}+\delta_l^2\,\frac{\partial v}{\partial x}\right)\right]\right\} \qquad (12)$$

$$\left(\mathrm{Re}_l\,\delta_l^2\right)\left(\frac{\partial w}{\partial t}+u\,\frac{\partial w}{\partial x}+v\,\frac{\partial w}{\partial y}\right)+\;u\,\frac{dr}{dx}-\delta_l v\,\sqrt{1-\left(\frac{dr}{dx}\right)^2}\;=\frac{\partial}{\partial y}\left(\mu_l\,\frac{\partial w}{\partial y}\right)+\delta_l^2\,\frac{\partial}{\partial x}\left(\mu_l\,\frac{\partial w}{\partial x}\right) \qquad (13)$$

$$\frac{\partial\theta}{\partial t}+u\,\frac{\partial\theta}{\partial x}+\left(\frac{\delta_l}{e_l}\right)v\,\frac{\partial\theta}{\partial y_T}\;=\left(\frac{1}{\mathrm{Pr}_l\,\mathrm{Re}_l\,e_l^2}\right)\left(\frac{\partial^2\theta}{\partial y_T^2}+e_l^2\,\frac{\partial^2\theta}{\partial x^2}\right)+(E)\left[2\delta_l^2\left(\frac{\partial u}{\partial x}\right)^2+2\delta_l^2\left(\frac{\partial v}{\partial y}\right)^2\right.$$

$$\left.+\,2\delta_l^2\,\frac{\partial u}{\partial y}\,\frac{\partial v}{\partial x}+\left(\frac{\partial u}{\partial y}\right)^2+\delta_l^3\left(\frac{\partial v}{\partial x}\right)^2+\left(4\mathrm{Re}_\Omega^2\,\delta_l^4\right)\left(\frac{\partial w}{\partial y}\right)^2+\left(4\mathrm{Re}_\Omega^2\,\delta_l^6\right)\left(\frac{\partial w}{\partial x}\right)^2\right] \qquad (14)$$

A list of the equation parameters and their values for a possible test material at a condition of interest is presented in table I. Physical properties used in computing values for table I are given in table II. Examination of the parameters reveals some which are not in common usage in the scientific community, and, therefore, warrant description:

N_p ratio of pressure driving effects to viscous retarding effects, will be referred to as pressure parameter

N_s may be interpreted as the ratio of centrifugal inertia effects to viscous effects, and , essentially, is a modified form of a Taylor number

g modified form of reciprocal Froude number

E modified form of Eckert number

The ratio N_s/N_p, therefore, relates the importance of centrifugal driving effects to pressure driving effects in the liquid layer.

TABLE I. - TYPICAL PARAMETERS FOR 650 OIL AND TEKTITES

Parameters	Material	
	650 Oil[a]	Tektite
Liquid Reynolds number, Re_l	3.04×10^{-3}	3.82×10^{-3}
Rotation Reynolds number, Re_Ω	$1.97\times10^{-1}\ \omega$	$0.42\times10^{-2}\ \omega$
Liquid scaling parameter for direction perpendicular to liquid-vapor interface, δ_l	0.5×10^{-1}	0.71×10^{-1}
Modified Taylor number, N_s	$3.19\times10^{-2}\ \omega^2$	$2.3\times10^{-5}\ \omega^2$
Dimensionless pressure parameter, N_p	7.5	1.18
Liquid thermal layer thickness, e_l	0.665×10^{-1}	1.27×10^{-1}
Liquid Prandtl number, Pr_l	3.95×10^{4}	2.85×10^{4}
Modified Eckert number, E	1.08×10^{-6}	7.35×10^{-6}
Dimensionless acceleration parameter, g	-1.19	-0.43

[a]Values are based on a model of 10^{-1} ft (3.05 cm) radius in a wind tunnel for an air velocity of 45 ft/sec (1.37 m/sec). The tektite calculations are based on estimated entry conditions as outlined in appendix B of ref. 8.

Order-of-magnitude analysis. - An order-of-magnitude analysis based on the values for the parameters contained in table I results in the following simplified equations:

$$\frac{\partial}{\partial x}(ru) + \frac{\partial}{\partial y}(rv) = 0 \tag{15}$$

$$\frac{\partial p}{\partial x} - g\sqrt{1 - \left(\frac{dr}{dx}\right)^2} - \left(\frac{N_s}{N_p}\right) r \frac{dr}{dx} = \left(\frac{1}{N_p}\right) \frac{\partial}{\partial y}\left(\mu_l \frac{\partial u}{\partial y}\right) \tag{16}$$

TABLE II. - PROPERTIES OF 650 OIL, AIR, AND TEKTITES

Property	Substance			
	650 Oil	Air		Tektites
Temperature properties evaluated at-				
^{o}F	60	78	5300	3040
^{o}K	289	299	3203	1943
Thermal conductivity, k:				
Btu/(ft)(sec)(^{o}F)	3.3×10^{-5}	4.16×10^{-6}	9.25×10^{-5}	2.57×10^{-4}
J/(m)(sec)(^{o}K)	2.05×10^{-1}	2.59×10^{-2}	5.75×10^{-1}	1.6
Specific heat, C_p:				
Btu/(slug)(^{o}F)	14.9	7.7	36.8	7.35
J/(kg)(^{o}K)	5.95×10^{2}	3.1×10^{2}	1.48×10^{3}	2.96×10^{2}
Density, ρ:				
slug/ft^3	1.73	2.3×10^{-3}	10^{-6}	4.65
kg/m^3	8.9×10^{2}	1.185	5.15×10^{-4}	2.4×10^{3}
Viscosity, μ:				
slug/(ft)(sec)	0.88×10^{-1}	0.39×10^{-6}	1.61×10^{-6}	1.00
kg/(m)(sec)	4.22	1.87×10^{-5}	7.72×10^{-5}	4.79×10^{1}
Melting temperature:				
^{o}F	15	---	---	1500
^{o}K	264	---	---	1089
Source	Ref. 9	Standard conditions	Ref. 11	Ref. 8

$$\frac{\partial p}{\partial y} + \left(\delta_l \frac{N_s}{N_p}\right) r \sqrt{1 - \left(\frac{dr}{dx}\right)^2} = 0 \tag{17}$$

$$u \frac{dr}{dx} = \frac{\partial}{\partial y}\left(\mu_l \frac{\partial w}{\partial y}\right) \tag{18}$$

$$\frac{\partial \theta}{\partial t} + u \frac{\partial \theta}{\partial x} + v \frac{\partial \theta}{\partial y} = \left(\frac{1}{\beta}\right) \frac{\partial^2 \theta}{\partial y^2} \tag{19}$$

$$\mu_l = \theta^{-N} \tag{20}$$

where $\beta = Pr_l Re_l \delta_l^2$ and relates the importance of convection effects to conduction effects.

These equations are the same as those obtained by Chen with the addition of centrifugal inertia terms in the equations of motion. The presence of these terms is illustrated in figure 2 by a force diagram. It is evident that in the meridional direction X, the centrifugal force aids in driving the liquid along the surface. For a spherical body, the effect would be negligible at the stagnation point because of the dependence of the centrifugal force on distance R from the rotation axis and at the equator because of the geometry of the body $dR/dX = 0$. The maximum driving effect would occur at a position equidistant from these two minimum points. It should be noted that the centrifugal force, which is also a body force, acts in the opposite meridional direction compared with the deceleration force. Therefore, for high rotation rates, at some meridional positions, the centrifugal force may become sufficiently large to offset or overpower the deceleration force and its effects on the dynamics of the melt layer.

Governing Gas Equations

The problem of an axial airstream flowing over a rotating axisymmetric body has been treated by Schlichting in reference 12. An analytical investigation yielded boundary-layer parameters, frictional drag, and torques as a function of the ratio of circumferential velocity to free-stream velocity. The results for the case of a spherical body indicate that, for spin rates pertinent to this work, the momentum loss thickness, torque, and frictional drag are negligibly affected by rotation. Effects of rotation on the heat transfer from a body of revolution in an axial airstream has been studied experimentally by Lewis and Ruggeri (ref. 13). Their results indicate that, for tangential velocities up to 105 feet per second (32 m/sec) and free-stream velocities of approximately 250 miles per hour (112 m/sec), no significant change in the heat-transfer coefficients occurred.

It is evident, therefore, that, for the problem at hand, the governing equations for the gas may be approximated with little error by those for air flowing over a nonrotating body. This formulation has been accomplished by Chen whose equations, in ordered form, are presented here for the sake of completeness:

$$\frac{\partial}{\partial x}(ru) + \frac{\partial}{\partial y}(rv) = 0 \tag{21}$$

$$u \frac{\partial u}{\partial x} + v \frac{\partial u}{\partial y} = - \frac{\partial p}{\partial x} + \frac{\partial^2 u}{\partial y^2} \tag{22}$$

$$\frac{\partial p}{\partial y} = 0 \tag{23}$$

$$u \frac{\partial \theta}{\partial x} + v \frac{\partial \theta}{\partial y} = \left(\frac{1}{Pr_g} \right) \frac{\partial^2 \theta}{\partial y^2} \tag{24}$$

Tektite Parameters

Because the ordering procedures were carried out for a specific test material and conditions, it is of interest to compare the calculated parameters with those obtained for a tektite entering the atmosphere. This has been done in table I for estimated entry conditions as presented in reference 8. Physical properties of air and tektites for these conditions are shown in table II. Comparison of the terms in table I indicates that, with the exception of the rotation parameters Re_Ω and N_s, the values of a parameter for 650 oil and tektites are of the same order of magnitude.

EXPERIMENTAL APPARATUS

Test Model

The characteristics deemed desirable in the material composing the model were

(1) That its viscosity be highly dependent on temperature

(2) That it have a relatively high specific heat and low thermal conductivity

(3) That its melting point be relatively low

This last characteristic was particularly advisable in that it removed the necessity for a high-temperature aerodynamic facility. The material chosen was 650 oil, the properties of which were given earlier in table II.

The oil was formed on the exterior of a 1.1-inch- (2.8-cm-) diameter wooden sphere. Attached to the sphere was a 0.375-inch- (0.95-cm-) diameter, 3-inch- (7.62-cm-) long plastic tube. These materials were chosen to minimize conduction away from the oil through its supporting structure. The method used to form the oil on the wooden sphere was developed by Chen (ref. 9). By alternately dipping the sphere in oil and liquid nitrogen, thin layers of solidified oil were built up until the desired size was reached

(approximately 2 in. (5.08 cm) in diam). Figure 3 schematically shows the details of the model.

Temperature within the model was measured by a copper-constantan thermocouple located adjacent to the wooden sphere and on the major axis of the model.

Aerodynamic Facility

To simulate deceleration through the atmosphere, the experiments were conducted in a vertical air duct. This wind tunnel was designed by Chen and is shown in figure 4. A centrifugal blower, driven by a 7.5-horsepower (5580-W) induction motor, forced room-temperature air through the tunnel at approximately 45 feet per second (13.7 m/sec). As illustrated in the schematic drawing, guide vanes, baffles, and screens were used to reduce the turbulence level in the flow and provide a flat velocity profile in the vertical portion of the tunnel. The ducting was constructed of sheet metal with the exception of one section which was clear plastic so that the ablating model could be

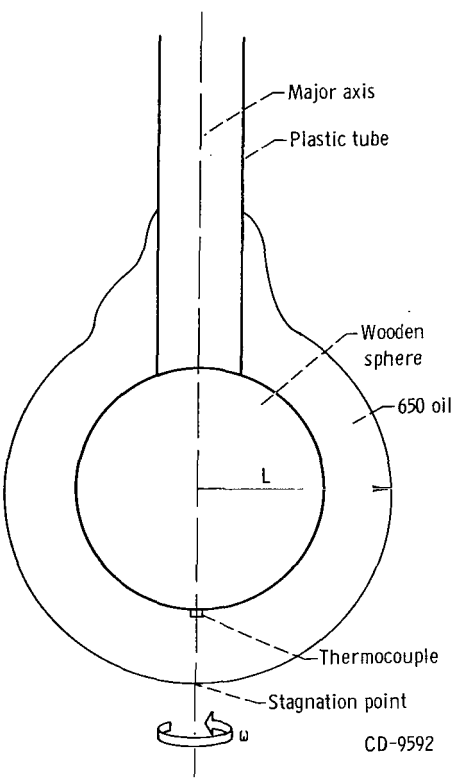

Figure 3. - Test ablation model.

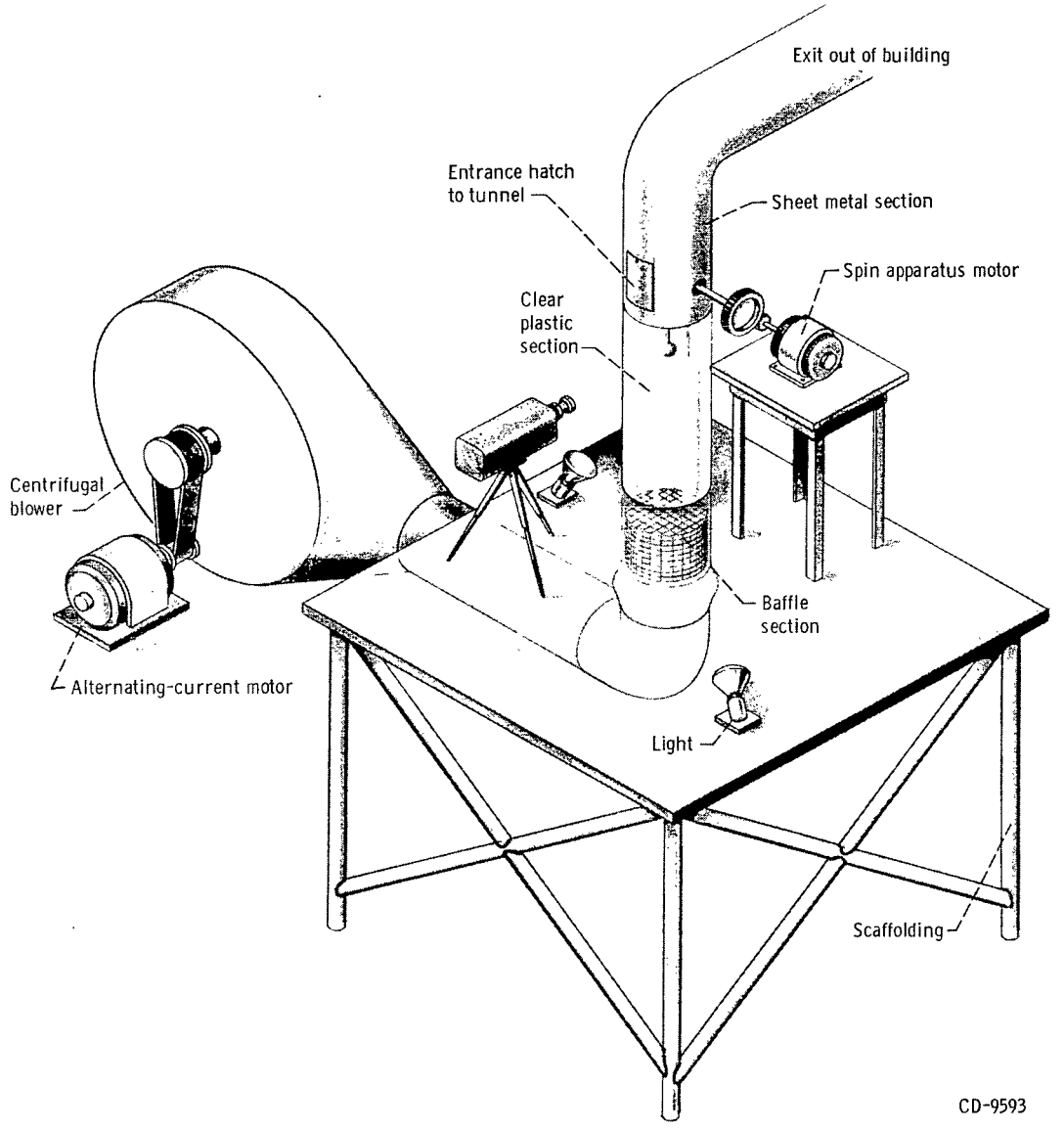

Figure 4. - Aerodynamic facility.

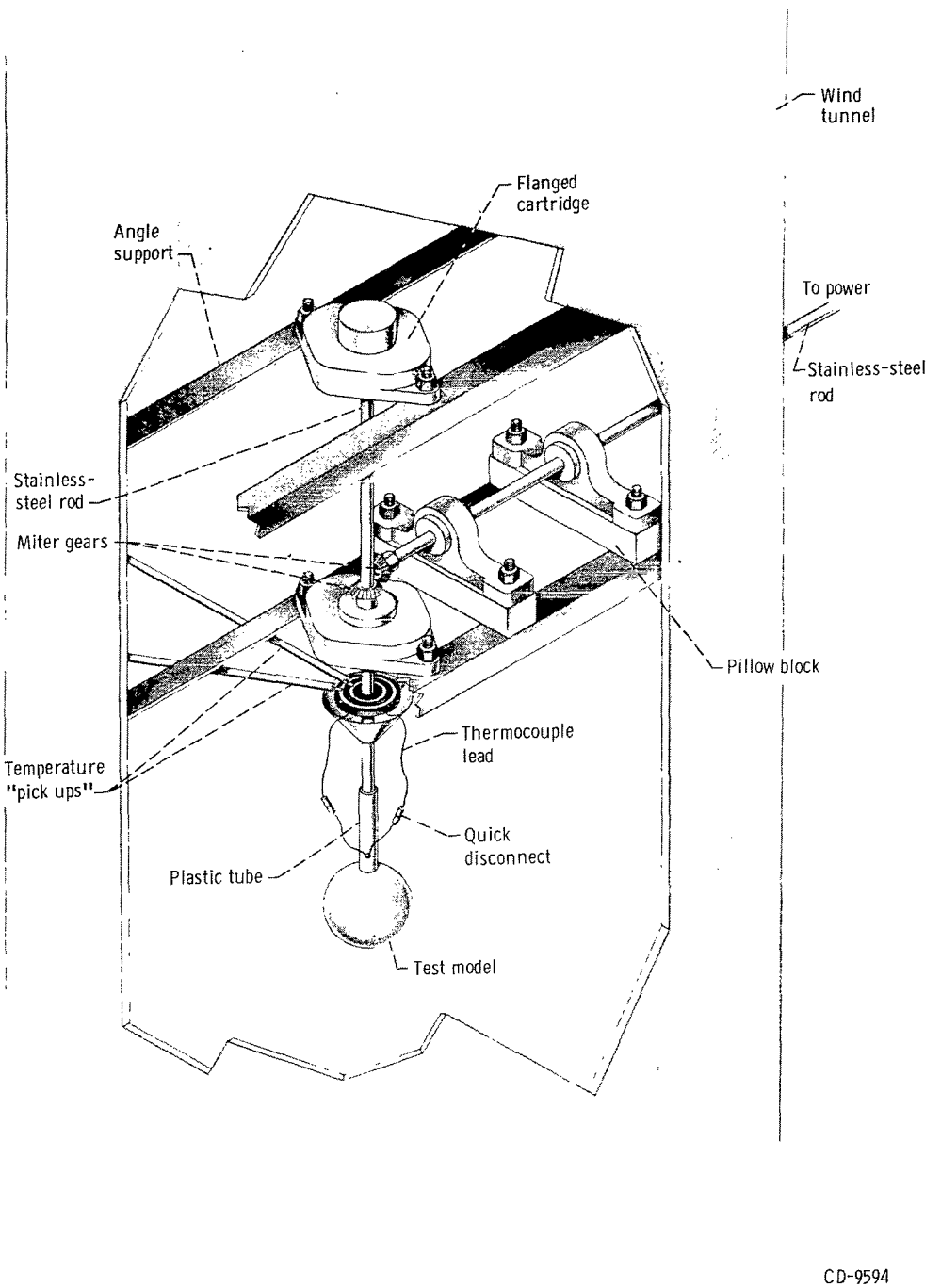

Figure 5. - Spinning apparatus.

observed and photographed. Motion pictures were taken with a 16-millimeter camera that was electrically driven at 25 frames per second. Illumination was supplied by two photoflood lights. Time reference was provided by a digital clock mounted outside the tunnel in the field of view of the camera.

Apparatus to spin the models was installed in the tunnel as shown in figure 5. A 1/15-horsepower (0.496-W) variable-speed direct-current motor provided the driving force through a system of gearing. At the motor end of the power train, worm gearing was used for the slower rotation speeds, while a system of spur gears was used to attain faster rates. The speed of the motor was checked under test conditions with a stroboscope and varied a maximum of $1\frac{1}{2}$ percent.

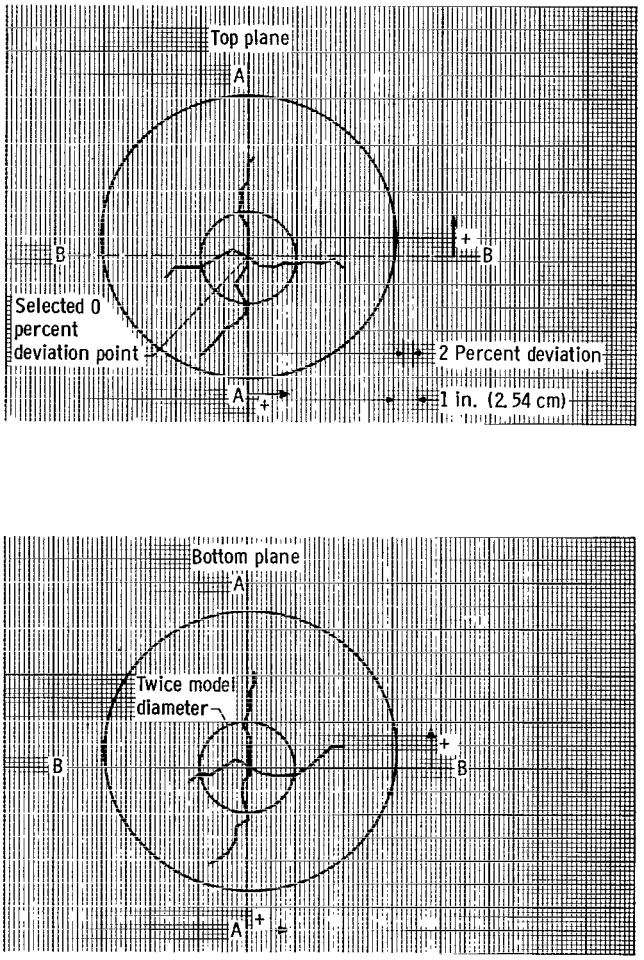

Figure 6. - Velocity profiles in wind tunnel.

The test models were fixed on the spinning apparatus by slipping the plastic tube over the end of the vertical shaft and shoving upward until a firm friction fit was effected. Leads from the thermocouple were connected to two slip rings, one copper and one constantan. Brushes rode on the rings and enabled the model temperature to be recorded on a paper chart recorder which operated at a constant speed. The cold junction was maintained at 32° F (273° K).

Preliminary Testing

After the apparatus to spin the models was installed in the tunnel, velocity profiles were obtained in the A-A and B-B directions, which are shown in figure 6. This was done in planes immediately above and below the test model location to ensure that the airflow was not being adversely affected in the vicinity of the model. Measurements were made with a pitot tube which could traverse 10 inches (25.4 cm) into the tunnel. Pressure was recorded on a micromanometer that was "zeroed" at barometric conditions. The results are plotted in figure 6. It should be noted in this figure that the grid assumes a double role: (1) distance and (2) percent deviation of the velocity from that measured at a particular position. This position was selected in the top plane of measurement on what was the major axis of the model when it was installed on the spinning apparatus. The curves show that, within a distance of 2 inches (4.08 cm) from the major axis of the model, the air velocity varied a maximum of ±2 percent.

Turbulence intensity at the center of the test section was measured with a hot wire anemometer and found to be ±0.1 percent. Air temperature in the tunnel was measured with a copper-constantan thermocouple and recorded on a chart recorder.

TEST PROCEDURES AND DATA ACQUISITION

Procedures

After a model had been made, it was placed in a constant temperature bath. The bath consisted of a Dewar half filled with liquid nitrogen and covered with a heavy cloth. The model was suspended in the top half of the Dewar from a laboratory stand, and the thermocouple leads were attached so that the temperature in the model could be monitored on the chart recorder. After 5 to 10 minutes in the bath, the temperature decrease became slow (approximately 0.5 F°/min (0.28 K°/min)). In his experimental work, Chen (ref. 9) used a model with thermocouples at various positions in the oil and found

that fairly uniform conditions were attained after 5 minutes in the bath. When these approximate equilibrium conditions were attained,

(1) The model was removed from the bath and placed in the wind tunnel.

(2) The spinning rate was set at the desired speed and the blower started.

(3) Motion pictures were taken intermittently during the test which generally required about 15 minutes. Time scales were checked and correlated by occasionally recording the digital timer reading on the chart recorder.

(4) When all the oil had been ablated from the wooden sphere, the model was removed from the tunnel, and pressure measurements were made with a pitot tube.

Data Reduction

The zero point on the time scale was chosen as that time when the model was fixed on the spinning apparatus in the wind tunnel. This was exactly determined from the chart recorder because the model thermocouple started to "read out" at this point.

Analysis of the film was accomplished on a motion-picture analyzer that magnified the image eight times. Step by step film advance and vernier scales permitted accurate measurements to be made. In addition to observing the general ablation process, recession of the stagnation point and wave crest motion were determined. Also, profiles of the models were obtained by projecting the film onto paper and tracing the basic model outline (waves were not included).

Calculation of the pertinent nondimensional parameters for each test required, first, that the characteristic values for the variables be determined. Initially, the interface temperature T_i and the liquid viscosity at the interface $\overline{\mu}_{i\ell}$ were obtained by a trial-and-error solution of equations (B21) and (B22). This involved selecting a value of T_i from which a value of $\overline{\mu}_{i\ell}$ could be obtained from the viscosity-temperature data of Edling (ref. 10). The value for $\overline{\mu}_{i\ell}$ was then inserted into equations (B24) and (B25), and a value for T_i was calculated. The procedure was continued until the assumed and calculated values of T_i were the same. The remainder of the characteristic values could then be obtained from their formulation as presented in appendix B.

RESULTS AND DISCUSSION

Test Conditions and Parameters

A summary of the test condtions and equation parameters for the experimental runs is presented in table III. It can be seen that all the major parameters in the momentum

TABLE III. - TEST CONDITIONS AND PARAMETERS

[Gas Prandtl number, 0.72.]

Condition or parameter	Experimental run						
	1	2	3	4	5	6	7
Rotation rate, ω, rad/sec	0	1.51	8.2	13.5	19.4	30	42.6
Gas free-stream temperature, $T_{-\infty}$:							
^{o}F	77.8	77.8	77.8	76.8	76.8	76.8	76.8
^{o}K	298.6	298.6	298.6	298.0	298.0	298.0	298.0
Gas free-stream velocity in X-direction, $U_{-\infty}$:							
ft/sec	46	45.6	45.6	45.2	45.2	45.2	44.7
m/sec	1.40	1.39	1.39	1.38	1.38	1.38	1.36
Center-of-model temperature, T_{∞}:							
^{o}F	-1.5	-2.6	-0.2	-4.0	-5.2	-0.2	-0.2
^{o}K	254.5	253.9	255.3	253.2	253.1	255.3	255.3
Length characteristic of model size, L:							
ft	0.082	0.082	0.076	0.076	0.079	0.078	0.078
m	0.025	0.025	0.023	0.023	0.024	0.024	0.024
Gas Reynolds number, Re_g	2.10×10^{4}	2.21×10^{4}	2.04×10^{4}	2.02×10^{4}	2.10×10^{4}	2.08×10^{4}	2.06×10^{4}
Liquid Prandtl number, Pr_l	1.26×10^{5}	1.34×10^{5}	1.18×10^{5}	1.42×10^{5}	1.51×10^{5}	1.34×10^{5}	1.34×10^{5}
Ablation parameter, γ	0.530	0.526	0.542	0.510	0.500	0.526	0.526
Liquid interface viscosity, μ_{il}:							
slug/(ft)(sec)	0.282	0.298	0.263	0.316	0.334	0.298	0.298
kg/(m)(sec)	13.5	14.3	12.6	15.2	16.0	14.3	14.3
Interface temperature, T_i:							
^{o}F	50.25	50.00	50.50	49.75	49.50	50.00	50.00
^{o}K	283.3	283.2	283.4	283.0	282.9	283.2	283.2
Reference velocity in X-direction, U_{ref}:							
ft/sec	0.76×10^{-3}	0.70×10^{-3}	0.82×10^{-3}	0.67×10^{-3}	0.62×10^{-3}	0.72×10^{-3}	0.71×10^{-3}
m/sec	2.36×10^{-4}	2.14×10^{-4}	2.50×10^{-4}	2.04×10^{-4}	1.89×10^{-4}	2.20×10^{-4}	2.16×10^{-4}
Liquid scaling parameter for direction perpendicular to liquid-vapor interface, δ_l	0.0827	0.0794	0.0854	0.0848	0.0817	0.0846	0.0852
Time characteristic value, σ	1.02×10^{2}	1.17×10^{2}	0.93×10^{2}	1.13×10^{2}	1.28×10^{2}	1.08×10^{2}	1.10×10^{2}
Convection parameter, β	0.325	0.280	0.354	0.284	0.254	0.312	0.315
Absolute value of dimensionless acceleration parameter, g	0.93	0.94	0.88	0.90	0.93	0.92	0.94
Dimensionless pressure parameter, N_p	12.0	11.8	12.2	12.0	11.9	12.2	12.2
Dimensionless spinning parameter, N_s	0	0.066	1.74	4.7	10.5	24.6	51.0
Spin parameter, N_s/N_p	0	0.001	0.14	0.40	0.88	2.20	4.20

equations were kept relatively constant except the Taylor number N_s, thus permitting a clear picture of rotation effects to be obtained. The spin parameter N_s/N_p ranged from 0 to 4.2 (ω = 0 to 400 rpm) while the pressure parameter N_p and reciprocal Froude number g were maintained at approximately 12 and -0.9, respectively.

General Observations

Wave motion. - The characteristics and motion of the generated waves were closely observed on the film analyzer. In the case of the stationary model, the waves initially formed concentrically about the stagnation point. As these waves moved back along the model surface, they generally broke up, with some portions of the waves moving faster than others. At large displacements from the stagnation point, the waves were, in general, highly distorted, having lost their axisymmetric nature entirely. This is shown for typical waves in the photographs in figure 7(a).

For the rotating models, the waves again initially formed concentrically about the stagnation point and broke up as they moved back along the surface. However, it became evident that, as the rotation rate was increased and at large meridional X displacements, the waves were more axisymmetric. As shown in figure 7(b), the waves had the shape of a helix of one revolution. It is apparent, therefore, that the net effect of rotation was to make the waves more symmetric about the major axis of the model.

A possible cause for wave distortion was the imperfect velocity profile (±2 percent deviation from the stagnation point). To ascertain this effect, a test was conducted at a low rotation rate (14 rpm). For such a condition, the centrifugal effects would be small (N_s/N_p = 0.001), and the small discrepancies in the velocity profile should be evened out about the model. Observation of the data film revealed no significant change in the waves from those observed on the stationary model.

Wave amplitude. - Another change in the wave characteristics which was observed in the data films (see fig. 7) concerned the wave amplitude. It was apparent that the amplitude of the waves decreased as the rotation rate was increased. However, attempts to measure the reduction were fruitless because of the minuteness of the amplitude itself. An explanation for this reduction is concerned with the opposing centrifugal and deceleration forces in the melt layer, as has been discussed. Ostrach (ref. 14) indicates that the presence of a deceleration force in the melt layer results in the amplitude of the waves becoming greater. Therefore, by rotating the models and negating the deceleration effects with the centrifugal effects, it seems reasonable that the wave amplitude should decrease.

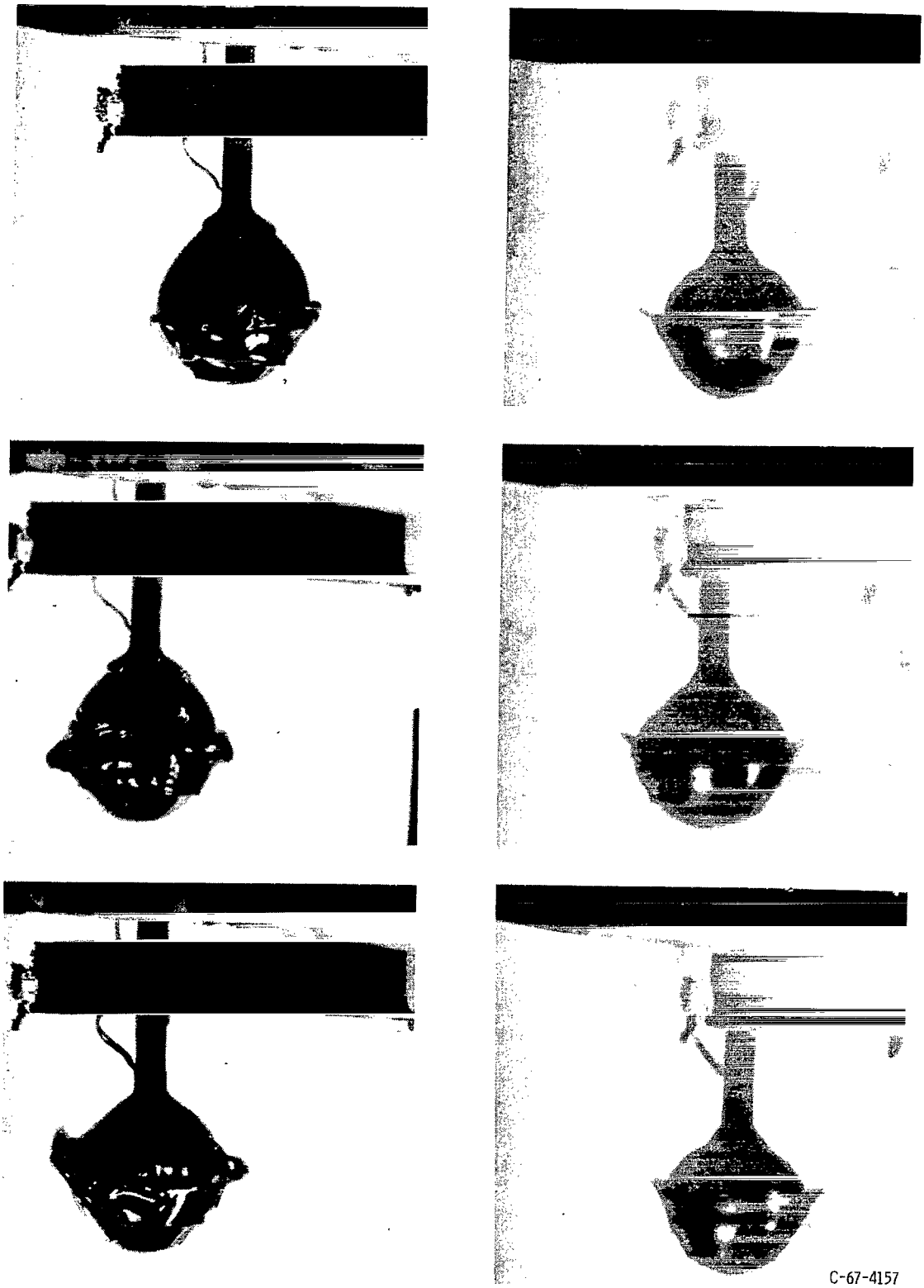

(a) Spin parameter, 0.

(b) Spin parameter, 4.2.

Figure 7. - Appearance of models during ablation.

Recession of Stagnation Point

The progress of the ablation process in the vicinity of the stagnation point may be determined by the recession of that point from its original position. This measurement was made for each of the test runs except run 3. During this test, the digital clock stopped for a period of time that could not be accounted for.

The results are presented in dimensional form in figure 8 and nondimensionally in figure 9. The shapes of the curves agree with the experimental and analytical results

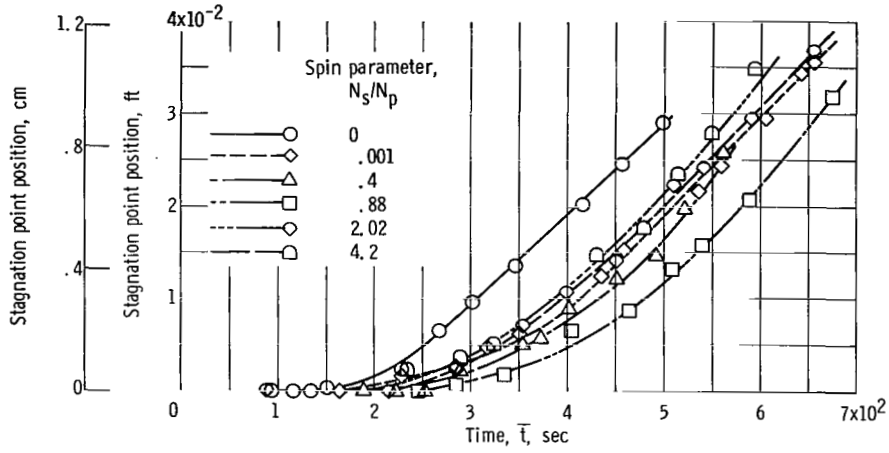

Figure 8. - Recession of stagnation point for various spin rates.

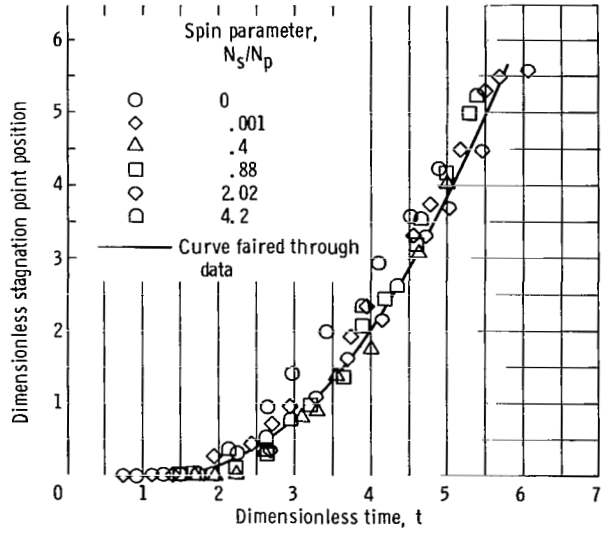

Figure 9. - Dimensionless recession of stagnation point.

of reference 8, that is, the ablation velocities, as indicated by the slopes of the curves, are small initially and approach a steady-state value after some time has elapsed. It is apparent from figure 9 that, with the exception of data from the stationary model, Chen's nondimensional technique correlated the results. The discrepancy in the results for the one test may well be accounted for by experimental error. Primarily, the conclusion to be drawn from these data is that no clear effect of rotation was noted in the recession of the stagnation point. This would be expected because of the dependence of centrifugal force on distance from the axis of rotation.

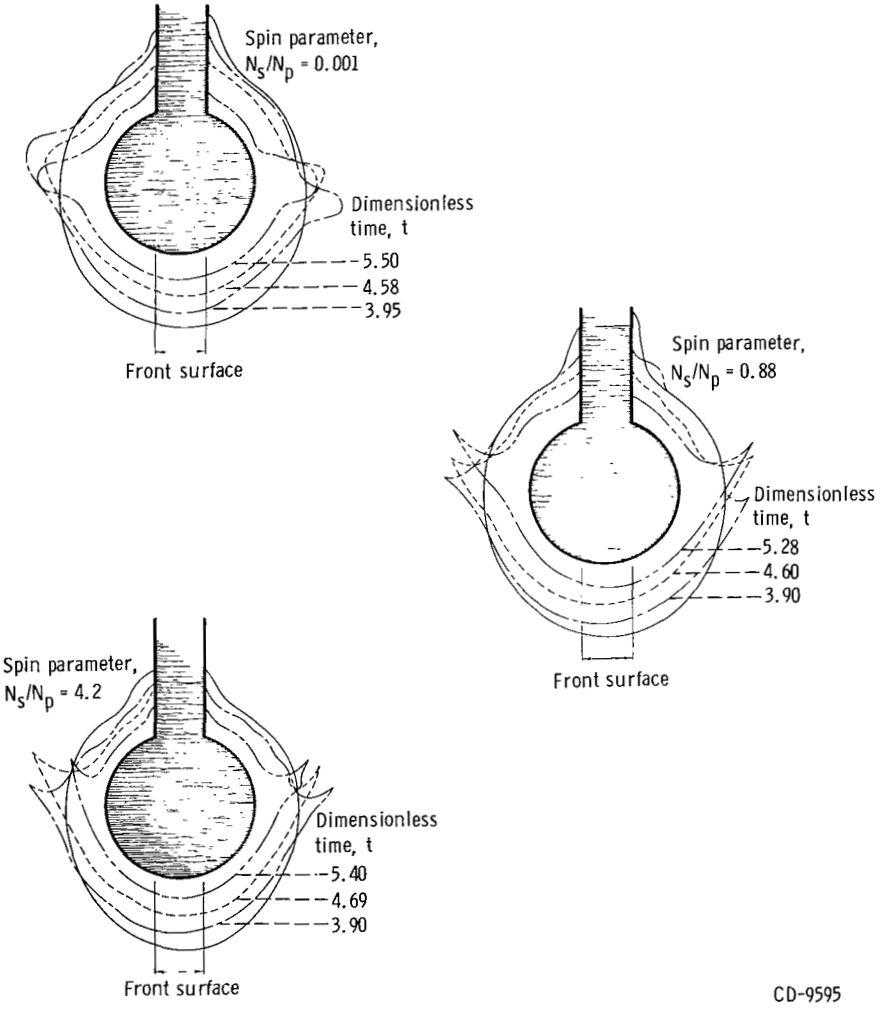

Figure 10. - Body shape at various spin rates and dimensionless times.

Body Shape Characteristics

Front surface. - In order to study further the effect of rotation on the ablation process in the vicinity of the stagnation point, the profiles of the models at various times were investigated, as indicated in Data Reduction. The results are presented in figure 10 for a cross section of the test conditions. What are considered to be the "front" surfaces of the models are denoted in the figure. This area was defined as being upstream of the meridional X inception point of the waves as generated on the stationary model. The need for this specification is brought out in a later discussion (see section, Wave Dynamics). Investigation of these front areas reveals that the surface shapes remained essentially spherical during the ablation process for all test conditions. Apparently, for the meridional displacements concerned, the centrifugal effects do not become large enough to affect the ablation process.

Flange. - A significant change that occurred in the body shape as a function of rotation rate was observed in the vicinity of the flange. It is shown in figures 7 and 10 that, for no rotation and small rates of rotation, the melted material accumulated in an unsymmetrical mass in the vicinity of the equator of the models. Occasionally, relatively large chunks of liquid were torn from this flange by the shearing effect of the airstream. At higher rotation rates ($N_s/N_p \geq 0.88$), the flange was swept back along the model surface because of the centrifugal effects acting normal to and along the liquid-vapor interface. In addition, liquid was propelled from the model in a small steady stream around the entirety of the flange.

Wave Dynamics

The effects of rotation on the ablation process in the vicinity of the stagnation region and flange having been investigated, attention was focused on the surface area between these positions by studying the motion of the generated waves. Consequently, the crest position of the waves as a function of time was measured for the different test conditions. The data for the test in which the spin parameter N_s/N_p equaled 0.001 were used instead of that from the stationary test because the entire circumference of the waves could be viewed in the former and not in the latter. Since the waves were not exactly axisymmetric, a maximum and minimum position at any one time was measured so that an average meridional X displacement could be determined. Waves were selected from that portion of the film when the models were ablating approximately at a constant rate, as determined from the stagnation point recession data ($t \geq 3.5$). Another prerequisite in selecting waves was that their entire lifetime from inception until they merged with

the flange be visible. Figures 11(a) to (f) present the results for the 28 waves measured. In these plots, each curve represents a different wave.

It is evident from the plots that there was scatter in the wave motion, particularly at large displacements. However, there are some effects of rotation apparent. The inception point of a wave was defined as being that meridional displacement at which the wave crest first appeared. If an average inception point is computed for each test condition, is normalized with respect to the model radius, and is plotted against the spin parameter N_s/N_p, figure 12 results. Here it can be seen that for higher rotation rates, the position where the crest of the waves is first observed occurs at larger distances from the stagnation point. The movement of this point to larger meridional X values is concerned with the role the deceleration force has in forming the waves. McConnell (ref. 8) states that "under heating and the action of the deceleration force, a small amount of melt accumulates on the forward portion of the body." Therefore, if the deceleration force is negated by centrifugal force, the inception point of the waves should be affected. The fact that the inception point of the waves changed with rotation rate necessitated the specification of the front surface to be based on the stationary model, as was indicated in a previous discussion.

Further inspection of the waves reveals that a period of time and distance is required for them to accelerate to the relatively large values of velocity they ultimately attain.

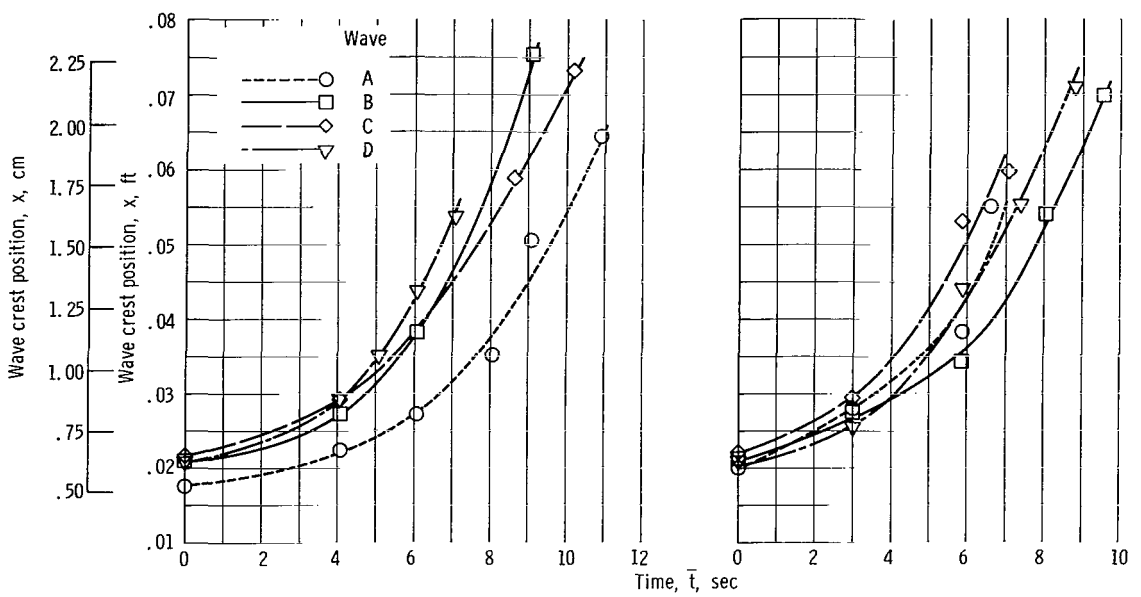

(a) Spin parameter, 0.001. (b) Spin parameter, 0.1.

Figure 11. - Wave crest position as function of time for various spin parameters.

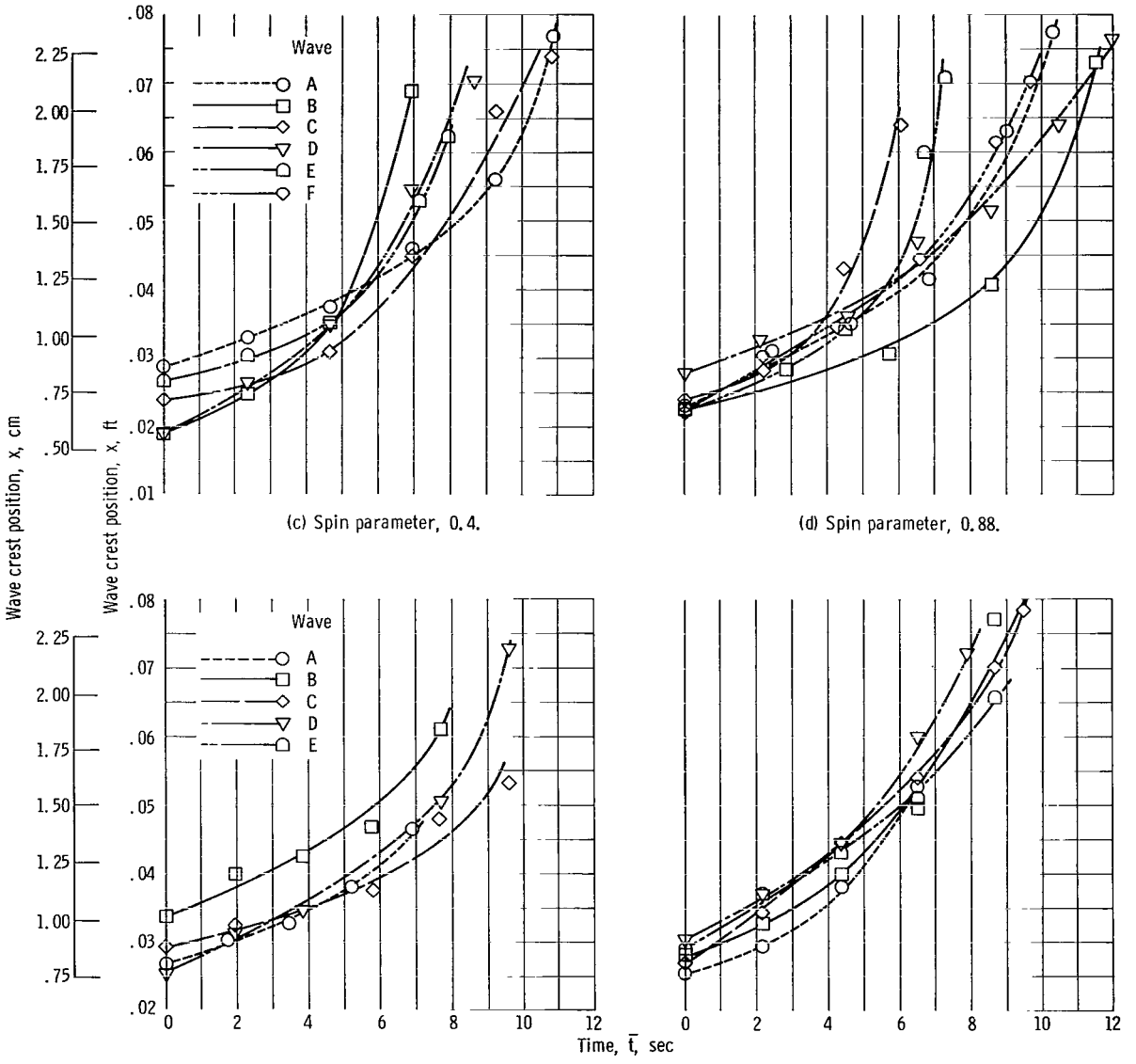

(c) Spin parameter, 0.4.

(d) Spin parameter, 0.88.

(e) Spin parameter, 2.02.

(f) Spin parameter, 4.2.

Figure 11. - Concluded.

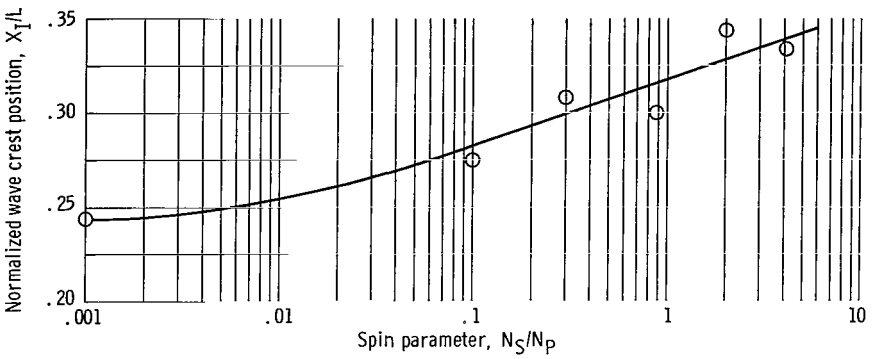

Figure 12. - Effect of rotation on wave inception.

Since the position of wave inception is delayed at larger rotations, the surface area over which large wave velocities are present is decreased. Therefore, because the "melt movement and the wave motion are fundamentally related" (ref. 8), the effectiveness of the air shearing force in driving the liquid layer should be reduced.

Temperature Rise of Body Fixed Point

The temperature data, as measured by the thermocouples in the models, are plotted dimensionally in figure 13 and nondimensionally in figure 14. The basic parabolic shape of these curves is in agreement with the experimental results of reference 8.

Investigation of figure 14 shows that the nondimensionalization did not correlate that data quite as well as it had the stagnation point recession results (fig. 9). It appears that the data for the runs in which the spin parameter equaled 2.02 and 4.2 are displaced a constant amount on the time axis from the remainder of the data. This would seem to indicate that the initial conditions for these two tests were different than for the others. A possible explanation is that small temperature gradients were present within these models, thus delaying the temperature increase in the vicinity of the thermocouple. These gradients could have been the result of the models manufacture because the length of time the models were inserted in the liquid nitrogen was not closely regulated. However, even if the data from these tests were displaced the proper amount to the left in the plot, there would still be some scatter. McConnell (ref. 8) had a comparable amount of scatter in his dimensionless temperature data so that the results of this work are not unusual in that respect.

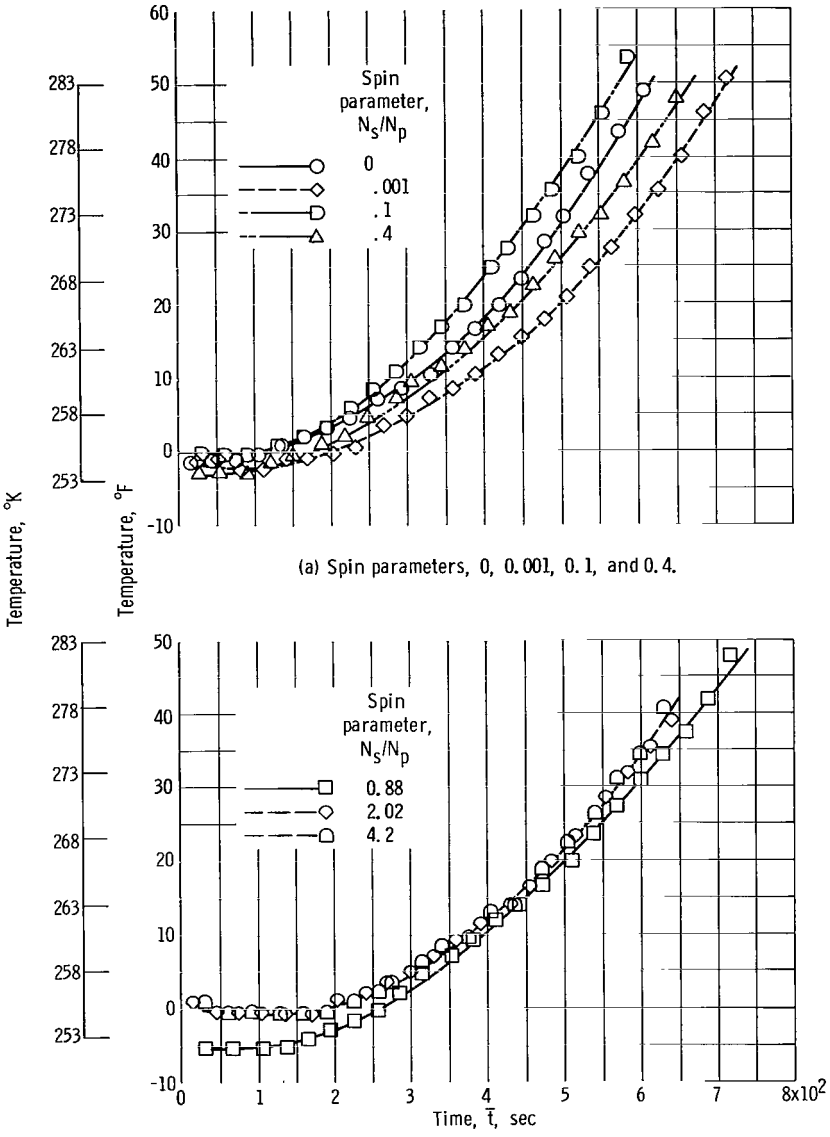

(a) Spin parameters, 0, 0.001, 0.1, and 0.4.

(b) Spin parameters, 0.88, 2.02, and 4.2.

Figure 13. - Temperature rise of body fixed point at various spin rates.

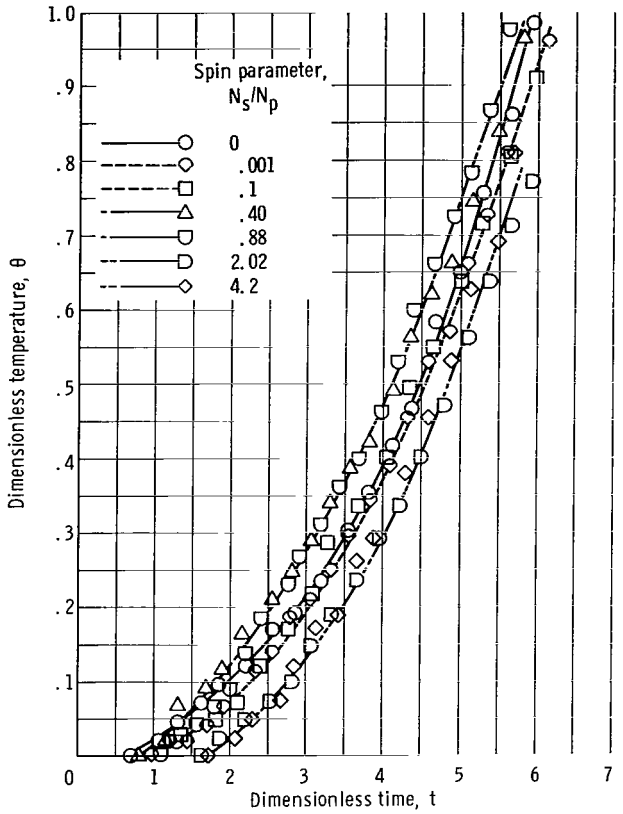

Figure 14. - Dimensionless temperature rise of body fixed point.

The conclusion of primary importance to be drawn from the data concerns that time during which steady-state ablation occurred. This period was characterized by the stagnation point receding at a constant rate. From figure 9, this is seen to occur approximately at dimensionless times greater than 3.5. From figure 14, it is apparent that during this time the slopes of the curves faired through the data are all about the same. Therefore, it must be concluded that the temperature rise of the thermocouple, and hence, the rate at which heat was transferred to the vicinity of the thermocouple, was not affected by rotation.

CONCLUDING REMARKS

The effects of rotation on the ablation of an axisymmetric body composed of a highly viscous material and subject to deceleration in an airstream were studied analytically

and experimentally. The tests were conducted so that a parameter representing the importance of rotation effects and which was obtained from a nondimensionalization of the governing equations was varied from 0 to 4.2. The following results were noted:

1. The recession of the stagnation points of the models was not affected by rotation.

2. Ablation in the vicinity of the stagnation point appeared to be unaffected by rotation.

3. The heat transfer to a body fixed point on the major axis of the models was not affected by rotation.

4. Liquid was propelled from the models in the vicinity of the flange when the spin parameter (N_s/N_p) equaled 0.88 or greater.

5. From observation of data film, it was apparent that the amplitude of the waves decreased as rotation rate increased.

6. The inception point of the waves tended to occur at larger distances from the stagnation point so that the surface area over which relatively large wave velocities occurred was smaller as the rotation rate increased.

7. Rotation caused the waves to become more axisymmetric in nature.

From these conclusions, it is apparent that the net effect of rotation on the ablation process for small meridional displacements was insignificant. This is understandable because of the smallness of the centrifugal force for these displacements. The temperature rise of the thermocouples also indicated that, over the lower portion of the forward surface of the models, rotation had no effect. At larger distances from the stagnation point, significant rotation effects on the characteristics of the waves and on the structure of the flange were apparent.

Application of these results to the tektite problem indicates that the insensitivity of the ablation process to rotation over the front surface supports Chapman's arguments concerning entry velocities and angles. For rotation to have an effect away from the stagnation region on an actual tektite, the spin parameter (N_s/N_p) is approximately 1 or the rotation rate equals 2160 rpm, a seemingly prohibitive rate.

Lewis Research Center,
National Aeronautics and Space Administration,
Cleveland, Ohio, November 29, 1967,
124-09-03-01-22.

APPENDIX A

SYMBOLS

A	acceleration
C_p	specific heat
E	modified Eckert number, $U_{ref}^2/(C_p)_l(T_i - T_\infty)\delta_l^2$
e	thermal layer thickness
F_ω	centrifugal force
$F_{\omega x}$	component of centrifugal force in meridional direction
$F_{\omega y}$	component of centrifugal force normal to liquid-gas interface
g	dimensionless acceleration parameter, $\rho_l AL/\rho_g U_{-\infty}^2$
H	interface wave function
k	thermal conductivity
L	length characteristic of model size
N	index in viscosity-temperature relation
N_p	dimensionless pressure parameter, $\rho_g U_{-\infty}^2 \delta_l^2 L/\overline{\mu}_{il} U_{ref}$
N_s	modified Taylor number, $\rho_l \omega^2 L^3 \delta_l^2/\overline{\mu}_{il} U_{ref}$
P	pressure
Pr	Prandtl number, $\mu C_p/K$
p	dimensionless pressure
Q	heat-transfer rate
R	radius of axisymmetric body
Re	Reynolds number, $\rho UL/\mu$
Re_Ω	rotation Reynolds number, $\rho_l \omega L^2/\overline{\mu}_{il}$
r	dimensionless radius of axisymmetric body
T	temperature
t	dimensionless time
$\overline{t}$	time
U	velocity in X-direction
u	dimensionless velocity in X-direction
V	velocity in Y-direction
v	dimensionless velocity in Y-direction
W	dimensionless velocity in $\overline{Z}$-direction
$\overline{W}$	velocity in $\overline{Z}$-direction
X	direction along liquid-vapor interface meridionally
x	dimensionless direction along liquid-vapor interface meridionally
Y	direction perpendicular to liquid-vapor interface
y	dimensionless direction perpendicular to liquid-vapor interface
$\overline{Z}$	direction along liquid-vapor interface azimuthally
z	dimensionless direction along liquid-vapor interface azimuthally

β	convection parameter $Re_l Pr_l \delta_l^2$
γ	ablation parameter
δ	scaling parameter for direction perpendicular to liquid-vapor interface
η	dimensionless interface wave function
θ	dimensionless temperature
μ	dimensionless viscosity
$\overline{\mu}$	viscosity
ρ	density
σ	time characteristic value
τ	shear stress
ω	rotation rate

Subscripts:

g	gas
I	wave inception
i	interface
l	liquid
m	melting point
o	stagnation point
ref	reference
T	thermal layer
∞	center of model
$-\infty$	gas free stream

APPENDIX B

SUMMARY OF CHEN'S ANALYSIS

Continuity Relation

The continuity equation in dimensionless form is

$$(U_{ref})\frac{\partial}{\partial x}(ru) + \left(\frac{\Delta_1 U_{ref}}{\delta_l}\right)\frac{\partial}{\partial y}(rv) = 0 \tag{B1}$$

Since continuity requires that these two terms be of the same order of magnitude

$$\Delta_1 = \delta_l \tag{B2}$$

Wave Motion Relation

The wave motion at the liquid-gas interface is described by

$$\frac{\partial H}{\partial \bar{t}} + U_i \frac{\partial H}{\partial X} - V_i = 0 \tag{B3}$$

where

$$Y = H(x, \bar{t}) \tag{B4}$$

In nondimensional form, equation (B3) becomes

$$\left(\frac{L}{\sigma U_{ref}}\right)\frac{\partial \eta}{\partial t} + u_i \frac{\partial \eta}{\partial x} - v_i = 0 \tag{B5}$$

where

$$\eta = \frac{H}{L\delta_l} \tag{B6}$$

Since a requirement for wave motion is that $\partial\eta/\partial t$ must be of the same order as the remaining terms,

$$\frac{L}{\sigma U_{ref}} \cong 1 \tag{B7}$$

Heat-Transfer Boundary Condition

From a consideration of the heat-transfer rate across the liquid-gas interface,

$$Q_i = -K_g \frac{\partial T}{\partial Y}\bigg|_{g_i} = -K_l \frac{\partial T}{\partial Y}\bigg|_{l_i} \tag{B8}$$

Nondimensionalizing results in

$$\left[\frac{K_g(T_{-\infty} - T_i)}{L e_g}\right] \frac{\partial\theta}{\partial y_T}\bigg|_{g_i} = \left[\frac{K_l(T_i - T_\infty)}{L e_l}\right] \frac{\partial\theta}{\partial y_T}\bigg|_{l_i} \tag{B9}$$

where

$$\theta\,\big|_g = \frac{T - T_i}{T_{-\infty} - T_i} \tag{B10}$$

and

$$y_T\,\big|_g = \frac{Y}{L e_g} \tag{B11}$$

since the two terms in equation (B9) must be of the same order of magnitude:

$$\frac{K_g(T_{-\infty} - T_i)}{e_g} \cong \frac{K_l(T_i - T_\infty)}{e_l} \tag{B12}$$

Shear Stress Boundary Condition

Equating the gas and liquid shear stress across the interface results in

$$\tau_i(x, \bar{t}) = \bar{\mu}_{gi} \left.\frac{\partial U}{\partial Y}\right|_{gi} = \bar{\mu}_{li} \left.\frac{\partial U}{\partial Y}\right|_{li} \tag{B13}$$

The corresponding nondimensional equation is

$$\left(\frac{\bar{\mu}_{gi} U_{-\infty}}{L\,\delta_g}\right) \left.\frac{\partial u}{\partial y}\right|_{gi} = \left(\frac{\bar{\mu}_{li} U_{ref}}{L\,\delta_l}\right) \left.\frac{\partial u}{\partial y}\right|_{li} \tag{B14}$$

The right and left sides of this equation are of the same order of magnitude so that

$$\frac{\bar{\mu}_{gi} U_{-\infty}}{\delta_g} \cong \frac{\bar{\mu}_{li} U_{ref}}{\delta_l} \tag{B15}$$

Liquid-Boundary-Layer Considerations

The energy equation (B14) provides a relation between the thermal and velocity layers in the body. In the steady state or long term, the amount of heat conducted into the body is of the same order of magnitude as that convected away in the moving layer. Therefore, it may be stated that

$$\frac{\delta_l}{e_l} \cong \frac{1}{Pr_l Re_l e_l^2} \tag{B16}$$

Chen provides a second relation between the thermal and velocity layers by assuming a linear temperature profile in the body or

$$\frac{\delta_l}{e_l} \cong \frac{T_i - T_m}{T_i - T_\infty} \tag{B17}$$

Gas-Boundary-Layer Considerations

The equations describing the heat-transfer and shear-stress relations between the liquid and gas at their interface inject two more unknowns into the problem; δ_g and e_g. These are determined from an order-of-magnitude analysis of the gas-boundary-layer equations.

From the gas momentum equation, in order for the viscous terms to be of 1 order of magnitude,

$$\delta_g \cong \left(\frac{1}{Re_g}\right)^{1/2} \tag{B18}$$

and from the gas energy equation

$$e_g \cong \frac{1}{(Re_g)^{1/2} Pr_g^m} \tag{B19}$$

where

$$m = 1 \text{ for } Pr_g > 1$$

$$m = \frac{1}{2} \text{ for } Pr_g < 1$$

Solution for Characteristic Quantities

The unknowns which remain in the problem are δ_l, U_{ref}, σ, e_l, and T_i. These are obtained by solving equations (B7), (B12), (B15), (B16), and (B17). The results are as follows:

Reference velocity:

$$U_{ref} \cong U_{-\infty} \left[\frac{(C_p)_l \, Pr_g^{(1-m)}}{(C_p)_g \, Pr_l}\right] \left(\frac{T_i - T_m}{T_{-\infty} - T_i}\right) \tag{B20}$$

Reference time:

$$\sigma = \left[\frac{LPr_l (C_p)_g}{U_{-\infty}(Pr_g)^{(1-m)} (C_p)_l}\right]\left(\frac{T_i - T_{-\infty}}{T_m - T_i}\right) \tag{B21}$$

Scaling parameter for liquid velocity layer thickness:

$$\delta_l \cong \left[\frac{K_l}{K_g(Pr_g)^m(Re_g)^{1/2}}\right]\left(\frac{T_i - T_m}{T_{-\infty} - T_i}\right) \tag{B22}$$

Scaling parameter for liquid thermal layer thickness:

$$e_l \cong \left[\frac{K_l}{K_g(Pr_g)^m(Re_g)^{1/2}}\right]\left(\frac{T_i - T_m}{T_{-\infty} - T_i}\right) \tag{B23}$$

Interface temperature:

$$\gamma^3 \cong \frac{T_{-\infty} - T_i^3}{(T_i - T_\infty)(T_i - T_m)^2} \tag{B24}$$

Ablation parameter:

$$\gamma = \left\{\left[\frac{K_l^2 (C_p)_l \rho_l \overline{\mu}_{gi}}{K_g^2 (C_p)_g \rho_g \overline{\mu}_{li}}\right]\frac{1}{Pr_g^{(3m-1)}}\right\}^{1/3} \tag{B25}$$

REFERENCES

1. Chapman, Dean R.; and Larson, Howard K.: On the Lunar Origin of Tektites. J. Geophys. Res., vol. 68, no. 14, July 15, 1963, pp. 4305-4358.

2. Ostrach, Simon; and McConnell, Dudley G.: Melting Ablation About Decelerating Spherical Bodies. AIAA J., vol. 3, no. 10, Oct. 1965, pp. 1883-1889.

3. O'Keefe, John A.: Tektites as Natural Earth Satellites. Science, vol. 133, no. 3452, Feb. 24, 1961, pp. 562-566.

4. O'Keefe, John A.; and Shute, Barbara: Tektites and Natural Satellites of the Earth. Paper No. 61-78, Institute of the Aerospace Sciences, Jan. 1961.

5. Adams, Mac C.: Recent Advances in Ablation. ARS J., vol. 29, no. 9, Sept. 1959, pp. 625-632.

6. Sutton, George W.: The Hydrodynamics and Heat Conduction of a Melting Surface. J. Aeron. Sci., vol. 25, no. 1, Jan. 1958, pp. 29-32.

7. Ostrach, Simon; Goldstein, Arthur W.; and Hamman, Jesse: The Effect of a Deceleration Force on a Melting Boundary Layer. J. Aeron. Sci., vol. 27, no. 8, Aug. 1960, pp. 626-627.

8. McConnell, Dudley G.: An Investigation of Transient Melting Ablation at the Surface of a Decelerating Spherical Body. Ph.D. Thesis, Case Institute of Technology, 1964.

9. Chen, C. J.: Melting Ablation of Two Dimensional and Axisymmetric Blunt Bodies With a body Force. Ph.D. Thesis, Case Institute of Technology, 1967.

10. Edling, Walter H.: An Experimental Study of Melting Wave Behavior. M.S. Thesis, Case Institute of Technology, 1966.

11. Hansen, C. Frederick.: Approximations for the Thermodynamic and Transport Properties of High-Temperature Air. NACA TN 4150, 1958.

12. Schlichting, H.: Laminar Flow About a Rotating Body of Revolution in an Axial Airstream. NACA TM 1415, 1956.

13. Lewis, James P.; and Ruggeri, Robert S.: Investigation of Heat Transfer from a Stationary and Rotating Ellipsoidal Forebody of Fineness Ratio 3. NACA TN 3837, 1956.

14. Ostrach, Simon: Melting Decelerating Bodies. Nonlinear Problems of Engineering. William F. Ames, ed., Academic Press, Inc., 1964, pp. 138-162.

NASA-Langley, 1968 —— 33 E-4049

NATIONAL AERONAUTICS AND SPACE ADMINISTRATION
WASHINGTON, D.C. 20546
OFFICIAL BUSINESS

FIRST CLASS MAIL

POSTAGE AND FEES PAID
NATIONAL AERONAUTICS AND
SPACE ADMINISTRATION

"The aeronautical and space activities of the United States shall be conducted so as to contribute . . . to the expansion of human knowledge of phenomena in the atmosphere and space. The Administration shall provide for the widest practicable and appropriate dissemination of information concerning its activities and the results thereof."

—NATIONAL AERONAUTICS AND SPACE ACT OF 1958

NASA SCIENTIFIC AND TECHNICAL PUBLICATIONS

TECHNICAL REPORTS: Scientific and technical information considered important, complete, and a lasting contribution to existing knowledge.

TECHNICAL NOTES: Information less broad in scope but nevertheless of importance as a contribution to existing knowledge.

TECHNICAL MEMORANDUMS: Information receiving limited distribution because of preliminary data, security classification, or other reasons.

CONTRACTOR REPORTS: Scientific and technical information generated under a NASA contract or grant and considered an important contribution to existing knowledge.

TECHNICAL TRANSLATIONS: Information published in a foreign language considered to merit NASA distribution in English.

SPECIAL PUBLICATIONS: Information derived from or of value to NASA activities. Publications include conference proceedings, monographs, data compilations, handbooks, sourcebooks, and special bibliographies.

TECHNOLOGY UTILIZATION PUBLICATIONS: Information on technology used by NASA that may be of particular interest in commercial and other non-aerospace applications. Publications include Tech Briefs, Technology Utilization Reports and Notes, and Technology Surveys.

Details on the availability of these publications may be obtained from:

SCIENTIFIC AND TECHNICAL INFORMATION DIVISION

NATIONAL AERONAUTICS AND SPACE ADMINISTRATION

Washington, D.C. 20546